Title
Fiber-based polarization-sensitive optical coherence tomography of a minimalistic system configuration.

Journal
Optics Letters, 44(12)

ISSN
0146-9592

Authors
Moon, Sucbei
Miao, Yusi
Chen, Zhongping

Publication Date
2019-06-15

DOI
10.1364/ol.44.003150

Peer reviewed

HHS Public Access

Author manuscript

Opt Lett. Author manuscript; available in PMC 2019 December 19.

Published in final edited form as:

Opt Lett. 2019 June 15; 44(12): 3150–3153. doi:10.1364/OL.44.003150.

Fiber-based polarization-sensitive optical coherence tomography of a minimalistic system configuration

SUCBEI MOON[1,2,†], **YUSI MIAO**[1,3,†], **ZHONGPING CHEN**[1,3,*]

[1]Beckman Laser Institute, University of California, Irvine, Irvine, California 92612, USA

[2]Department of Physics, Kookmin University, Seoul 02707, South Korea

[3]Department of Biomedical Engineering, University of California, Irvine, Irvine, California 92697, USA

Abstract

We present a very simple method of constructing a polarization-sensitive optical coherence tomography (PS-OCT) system. An ordinary fiber-based swept-source OCT system was reconfigured for PS-OCT by adding a long section of polarization-maintaining fiber in the sample arm. Two polarization modes of a large group-delay difference formed spatially distinguished polarization channels. The depth encoded information on the polarization states was retrieved by an amplitude-based analysis. We found that our method provides an economic scheme of PS-OCT. It demonstrates that an ordinary OCT system can be easily reconfigured for PS-OCT imaging if it has sufficient margins in the imaging range.

Polarization-sensitive optical coherence tomography (PS-OCT) provides a variety of opportunities in tissue imaging with its unique capability of acquiring depth-resolved sample birefringence or other polarization properties [1–4]. However, difficulties in system implementation and management are major obstacles in clinical applications. Bulk-optic construction of PS-OCT, frequently used in earlier development [5], is not compatible for a majority of fiber-optic technologies. Various techniques have been developed so far for fiber-based construction of PS-OCT systems with polarization-maintaining (PM) fibers or common single-mode (SM) fibers [6–8]. In one of the schemes [9,10], a swept-source OCT (SS-OCT) system based on SM fibers equips a passive delay unit (PDU) that produces polarization-dependent delays of the OCT signal. The PDU is made of bulk-optic elements or simply a long section of PM fiber. Detected by a pair of balanced photodetectors for polarization-channeled signal acquisition, full polarization information can be obtained with two polarization states incident on the sample in the PDU-based PS-OCT system. With help from auto-calibration techniques, such a system is designed to operate very robustly against systematic polarization variations. However, it requires a specialized design with added system complexity. There are several cost-effective approaches based on single cameras for spectral-domain OCT (SD-OCT) [11–13]. But they still require special configurations in the spectrometer designs or the synchronized operation of polarization modulators.

*Corresponding author: z2chen@uci.edu.

†These authors contributed equally to this work.

In many cost-sensitive applications, such an elegant but complicated approach is not available. There is a demand for low-cost and ready-to-use technologies that can take advantage of the present OCT systems while tolerating some incomplete features of simpler PS-OCT systems. Taking aim at those demands, we studied an economic scheme of re-configuring an ordinary OCT system to a PS-OCT variant. In our novel scheme, a long section of PM fiber is inserted at the sample arm of the OCT interferometer for polarization-dependent delays of a large retardation. The resulting OCT image contains a plurality of image replicas separated by the group delay difference of the polarization modes. The polarization-sensitive interference can be analyzed by the difference between the replicated images. With this scheme, any ordinary OCT system can be easily upgraded to add a useful PS-OCT imaging function if it supports a sufficiently long imaging range.

Constructing depth-encoded polarized detection channels for PS-OCT is not a novel approach [14]. Use of a long PM fiber or any type of PDU can be considered instead of using a pair of photodetectors arranged for different polarization channels. This requires a means of polarization controls that manages the input polarization state. It may unexpectedly increase system complexity. In Rivet *et al.* demonstration of a simple PS-OCT system [14], a bulk-optic module of a large retardation, was utilized for depth-encoded polarization detection. Their scheme, however, employs a polarizer in their passive optical module for a controlled polarization state, which complicates the optical design for non-reciprocal operation.

In this Letter, we report on a very simple method of PS-OCT system configuration based on a delay PM fiber. Figure 1 shows the schematic diagram of our PS-OCT system. It was based on an ordinary SS-OCT system operating at a center wavelength of 1.3 μm. A microelectromechanical system vertical-cavity surface-emitting laser (MEMS-VCSEL SL131090, Thorlabs Inc.) was used for the swept source. The full optical bandwidth was 100 nm. It provided a wide imaging range of 12 mm with low sensitivity roll-offs of less than 3dB. The system was operated at an A-line rate of 100 kHz with a signal sampling rate of 4.0 GS/s. The only modification we made to the previously constructed ordinary OCT system was to add a 12 m long PM fiber (PM1300-XP, Thorlabs Inc.) at the SM fiber's end of the sample arm. An SM fiber patch cable of the same length was inserted in the reference arm to match the optical path length. A quarter-wave plate (QWP) was placed right before the objective lens. Not shown in the figure, the clock signal output of the swept source was also delayed with a 30 m long coaxial cable. The purpose of using the long SM fiber patch cable and the coaxial cable delay was to match the overall signal delay. Those modifications of the system can be implemented with ease to any SS-OCT system. Note that the light of the swept source is assumed to be naturally polarized. Otherwise, a polarizer can be installed at the output of the light source.

The PM fiber utilized in our system is highly birefringent with two linearly polarized (LP) eigen-modes. As illustrated in Fig. 2(a), the light LP along the x axis (LPx) propagates faster than the light LP along the y axis (LPy) in the PM fiber. As a consequence, the OCT image obtained with the PM fiber in place produces repeated images. As depicted in Fig. 2(b), three replicated images can be generated by the roundtrip of the signal through the PM fiber. The fast-fast (FF) image is a result of the OCT signal delivered through LPx (fast) mode in

the roundtrip. The slow-slow (SS) image is produced through LPy (slow) mode in the roundtrip. And the fast-slow (FS) image is obtained from the OCT signal delivered through LPx (fast) mode in one way and LPy (slow) mode in the other way. The axial separation between the FF, FS, and SS images, denoted by Δz, equals one-way retardation of the PM fiber in the domain of axial delay, z. Here, Δz is determined by $\lambda \cdot L \cdot B$, where B is the beat length and L is the fiber length of the PM fiber. In our system, Δz was measured to be 2.7 mm with L = 12 m. In most cases, this amount of separation was sufficiently large enough to avoid spatial overlap of those three image segments.

The polarization composition of the signal returning from the sample can be analyzed if the polarization state input to the PM fiber is known. It is required to make the input state either LPx or LPy. In this Letter, the case of LPx input will be mainly considered. Then, the amplitude ratio of two replicated images can be interpreted as that of the different polarization states for the returning light. This way provides a simple method of polarization-multiplexed detection with a single detection channel.

In our scheme, the polarization controls required for a known input polarization state are accomplished by our preoperational setup procedure of the systematic polarization states. The sample-arm polarization controller (sPC) and the reference-arm PC (rPC) in our system are aligned to produce certain image responses. In our polarization setup procedure, an optical reflector, such as a mirror, is placed at the sample stage, since it exhibits no polarization dependence in its reflectance. Our alignment procedure involves the following steps:

Step 1—Adjust the sPC for minimizing the amplitude of the SS image. Then, the input and the output of the PM fiber are completely in the LPx state. The FF image becomes the brightest.

Step 2—Set the angle of the QWP to be 22.5° with respect to the x axis. Then, the reflected field recoupled to the PM fiber is equally distributed to the LPx state and the LPy state.

Step 3—Adjust the rPC for equalizing the amplitudes of the FF image and the FS image. Then, the reference field interferes with the sample fields in both polarization states equally. Note that the roll-off characteristic of the signal amplitudes is neglected here.

Step 4—Set the angle of the QWP to be 45° with respect to the x axis. Then, the sample-incident light is circularly polarized (CP). From the reflector, the sample field recoupled to the PM fiber is completely in the LPy state. The FF image becomes the darkest, while the FS image becomes the brightest. The system is ready to take PS-OCT images.

The angle of the QWP can be measured in reference to the geometry of the PM fiber. Or one can find the orientation of the x axis by which the QWP maximizes the amplitude of the FF image and minimizes that of the FS image after Step 1. Meanwhile, our polarization setup procedure discards the SS image by Step 1. The SS image has no chance to get non-zero intensity. One can take an alternative approach of discarding the FF image and setting the PM fiber output completely in the LPy state in Step 1. Then, the FF image must be replaced by the SS image in all the descriptions related to the polarization setup procedure.

The effect of introducing a PM fiber section in our system can be described in simple algebra. The QWP acts as a transformer of polarization states. The LPy states at the PM fiber end are transformed to CP states before the sample. For a single sample reflection, the sample-reflected field generated from the sample-incident CP light is a vectorial field composed of two orthogonal bases of CP states, $\hat{e}_1$ and $\hat{e}_2$. Its interference with the reference field, which occurs at the coupler, can be equivalently taken at the exit of the QWP. The equivalent reference field, E_r, is expressed by

$$\overrightarrow{E}_r(z) = \hat{e}_1 a_{r1} E(z) + \hat{e}_2 a_{r2} E(z), \tag{1}$$

where a_{r1} and a_{r2} are the amplitude coefficients of the CP components. Here, $E(z)$ is the normal field that originates from the E_s is expressed in the source light. Meanwhile, the sample field same way by

$$\overrightarrow{E}_s(z) = \hat{e}_1 a_{s1} E(z - z_0) + \hat{e}_2 a_{s2} E(z - z_0 - \Delta z), \tag{2}$$

where a_{s1} and a_{s2} are complex amplitudes of the CP components. Δz is the one-way retardation of the PM fiber, while z_0 is the common-mode delay of the sample fields to the reference, which is the relative sample position. The detected signal intensity is taken from the sum of those two fields by summing up $|E_r + E_s|^2$ for the two vectorial components. In the complex notation, the interference term of cross-correlation intensity, I_{int}, is obtained by

$$\begin{aligned} \frac{I_{\text{int}}}{2} = \text{Re}\{ & a_{r1}^* a_{s1} E^*(z) E(z - z_0) \\ & + a_{r2}^* a_{s2} E^*(z) E(z - z_0 - \Delta z) \}. \end{aligned} \tag{3}$$

Here, the superscripted asterisk (*) denotes the complex conjugate, and Re{} is the operation of taking the real part. The Fourier transform of I_{int} gives the spectral interferogram that is actually detected in SS-OCT. And its inverse-transform process gives the A-line profile of OCT imaging. Equation (3) suggests that it contains two replicated responses separated by Δz. For a large value of Δz, each can be spatially filtered for further processes without spatial overlaps.

The polarization evolution along the depth in a birefringent sample turns out to be a depth-dependent ratio of a_{s1} to a_{s2}. The first sample surface gives $a_{s2} = 0$ by the polarization setup. The phase retardation of the sample field, δ, is found by

$$\delta = \arctan(a_{s1}/a_{s2}) \tag{4}$$

for the signal roundtrip. As suggested by Eq. (3), the amplitude ratio of a_{s1} to a_{s2} can be found from I_{int} for a known ratio of a_{r1} to a_{r2}. By Step 3 of our polarization setup procedure, it is set up to be unity $(|a_{r1}| = |a_{r2}|)$. Therefore, the retardation can be retrieved from the power ratio of the two terms of Eq. (3)

Based on the theory given above, the image signal processing for our PS-OCT can be performed with the acquired A-line data. The A-line reflectance profile, denoted by $A(z)$, is obtained by absolutizing the inverse Fourier transform of the spectral interferogram. The FF image and re-shifted FS image are taken by $A(z)$ and $A(z+\Delta z)$, respectively. Here, one must take the frequency dependence of Δz, i.e., the differential dispersion into account. Numerical dispersion compensation can be applied to each image segment in a different mode. Hence, two A-line profiles of FF and FS images, A_{FF} and A_{FS}, are obtained, respectively, by

$$A_{\mathrm{FF}}(z) = |F^{-1}\{J_{\mathrm{int}}(k)\cdot D_{\mathrm{FF}}(k)\}|, \tag{5}$$

and

$$A_{\mathrm{FS}}(z+\Delta z) = |F^{-1}\{J_{\mathrm{int}}(k)\cdot D_{\mathrm{FS}}(k)\}|, \tag{6}$$

where $F\{\}$ and $F^{-1}\{\}$ denote Fourier transform and inverse Fourier transform, respectively. Here, J_{int} is the spectral interferogram that comes from $F\{I_{\mathrm{int}}\}$. D_{FF} and D_{FS} are dispersion compensation functions for the FF and FS image segments, respectively [15,16], and k is the wavenumber. D_{FF} can be optimized for the best response of A_{FF}, while D_{FS} can be for the best A_{FS}.

From the two A-line data given by Eqs. (5) and (6), the PS-OCT image data can be retrieved. The normal A-line profile, A_{norm}, is obtained by the norm of the A-line reflectance vector as

$$A_{\mathrm{norm}}(z) = \sqrt{A_{\mathrm{FF}}^2(z) + A_{\mathrm{FS}}^2(z)}, \tag{7}$$

which makes up a polarization-independent OCT image. In the condition of $|a_{r1}| = |a_{r2}|$, one can assume $|A_{\mathrm{FF}}|$ is proportional to $|a_{s1}|$, while $|A_{\mathrm{FS}}|$ is proportional to $|a_{s2}|$. The sample-induced phase retardation is found with the normal profile by

$$\delta(z) = \arcsin\left(\frac{A_{\mathrm{FS}}(z)}{A_{\mathrm{norm}}(z)}\right) = \arccos\left(\frac{A_{\mathrm{FF}}(z)}{A_{\mathrm{nom}}(z)}\right) \tag{8}$$

from the FF and FS image data. Compared to the formula of Eq. (4), the calculation of Eq. (8) is more robust in avoiding divided-by-zero errors. By the property of the absolute amplitudes, the measured sample-induced retardation ranges from 0° to 90°. The spatial derivative of $\delta(z)$ will give the strength of the sample birefringence.

We tested the accuracy of retardation measurement for our PS-OCT system. A thin birefringent plate was used with one-way retardation of ~110°. We found an error of ~5° in the retardation measurements. Meanwhile, PS-OCT imaging capability of our system was tested with a tissue sample of rabbit tendon, *ex vivo*, with muscle attached to the side. Figure 3(a) shows a raw OCT image. There, only the FF and FS image segments are shown for simplicity. The characteristic banding pattern was produced by the sample birefringence in each segment. This verified that the long PM fiber provided depth-encoded polarization channels in our PS-OCT system. To obtain reflectivity and retardation maps from the raw OCT image, two A-lines of $A_{\mathrm{FF}}(z)$ and $A_{\mathrm{FS}}(z+\Delta z)$ were prepared as given by Eqs. (5) and

(6). Each was compensated differently in dispersion by a numerical method. At each point of the image, A_{norm} and δ were calculated for reflectivity and retardation by using Eqs. (7) and (8), respectively. Finally, Figs. 3(b) and 3(c) show the reflectivity map of the normal OCT image and the image of the sample-field retardation, respectively. The effect of the sample birefringence is clearly visualized in the pseudo-color map in Fig. 3(c). The tendon and muscle parts are easily distinguished by different levels of birefringence. Owing to the simplicity of our amplitude-based analysis, we have succeeded in real-time imaging of reflectivity and retardation as demonstrated with Visualization 1 of the supplementary material.

In this study, we proposed and demonstrated a very simple configuration of PS-OCT. Any Fourier-domain OCT (FDOCT) system can be reconfigured by simply adding a long section of PM fiber or any type of a polarization-differentiating delay unit as long as it has a sufficiently long axial imaging range for depth-encoded detections. Our method seems very attractive and particularly useful for SD-OCT systems, which have technical difficulties in implementing polarization-channeled spectrometers in pairs. The minimum required axial imaging range of OCT for 2 mm PS-OCT imaging is roughly 6 mm for three image segments not to collide. An SD-OCT system with good spectral resolution can provide enough margins for multiplexed detection.

The polarization controllers were manually aligned in our polarization setup procedure. We have observed that the systematic polarization states are maintained for at least a few hours if all the fibers are kept in a stable environment. Even though our procedure can be easily performed, the manual operation needs improvements for convenient and reliable operation. One may notice that the sPC can be re-aligned any time even in the middle of imaging after Step 1 of our polarization setup procedure. As well, it can be automated with an electrically controlled PC, which is managed at the lowest amplitudes of the SS image in a closed-loop operation mode. On the other hand, alignment of the rPC requires a special condition made by Step 2 and can hardly be performed in the middle of an imaging operation. This brings the need for further improvement and study to produce fully automated operations.

Unlike most SM fiber-based systems, our PS-OCT system retains a fixed CP state at the sample incidence. Likewise, the axes of the polarization detections are also fixed by the PM fiber. This allows us to measure the absolute state of polarization for the sample field. We could take advantage of the amplitude based analysis, which is simpler and more robust. To retrieve full polarization information including the orientation of birefringence, the signal phases of the two polarization channels must be obtained as well. Even with very long fiber delays, previous studies suggest that proper signal processing can extract the phase-involved information for PS-OCT [9]. However, it can be achieved with added complexity in signal processing and system calibration. It is worth noting that the phase errors can be produced by different numerical dispersion compensations or image shifting in our scheme, especially involving errors in *k*-domain signal sampling that relate to inaccurate timing synchronization in an SS-OCT system [16] or erroneous spectral calibration in an SD-OCT system [17].

In summary, we proposed a very simple PS-OCT construction scheme with a long PM fiber utilized for depth-encoded polarization-multiplexed signal detection. An ordinary SS-OCT

system was easily upgraded by adding delay fibers and keeping a single balanced photodetector. A polarization setup procedure was developed to operate our system at desired polarization states. Phase retardation information was successfully obtained from a tissue sample. We believe that our method can be a practical alternative for applications that demand an economic way of constructing a PS-OCT system.

Supplementary Material

Refer to Web version on PubMed Central for supplementary material.

Acknowledgment.

Z. C. has a financial interest in OCT Medical Imaging Inc., which, however, did not support this work. S. M. is a visiting scholar supported by the National Research Foundation of Korea (NRF2018R1D1A1B07045449).

Funding. National Institutes of Health (NIH) (R01EY028662, R01HL-125084, R01HL-127271, U54-ES027698); Air Force Office of Scientific Research (AFOSR) (FA955017–1–0193).

REFERENCES

1. de Boer JF, Srinivas SM, Malekafzali A, Chen Z, and Nelson JS, Opt. Express 3, 212 (1998). [PubMed: 19384363]
2. de Boer JF, Srinivas SM, Park BH, Pham TH, Chen Z, Milner TE, and Nelson JS, IEEE J. Sel. Top. Quantum Electron. 5, 1200 (1999). [PubMed: 25774083]
3. de Boer JF, Milner TE, van Gemert MJ, and Nelson JS, Opt. Lett. 22, 934 (1997). [PubMed: 18185711]
4. de Boer JF, Hitzenberger CK, and Yasuno Y, Biomed. Opt. Express 8, 1838 (2017). [PubMed: 28663869]
5. Hee MR, Swanson EA, Fujimoto JG, and Huang D, J. Opt. Soc. Am. B 9, 903 (1992).
6. Guo S, Zhang J, Wang L, Nelson JS, and Chen Z, Opt. Lett. 29, 2025 (2004). [PubMed: 15455768]
7. Zhang J, Jung W, Nelson JS, and Chen Z, Opt. Express 12, 6033 (2004). [PubMed: 19488244]
8. Saxer CE, De Boer JF, Park BH, Zhao Y, Chen Z, and Nelson JS, Opt. Lett. 25, 1355 (2000). [PubMed: 18066215]
9. Baumann B, Choi W, Potsaid B, Huang D, Duker JS, and Fujimoto JG, Opt. Express 20, 10229 (2012). [PubMed: 22535114]
10. Ju MJ, Hong Y-J, Makita S, Lim Y, Kurokawa K, Duan L, Miura M, Tang S, and Yasuno Y, Opt. Express 21, 19412 (2013). [PubMed: 23938857]
11. Baumann B, Götzinger E, Pircher M, and Hitzenberger CK, Opt. Express 15, 1054 (2007). [PubMed: 19532333]
12. Cense B, Mujat M, Chen TC, Park BH, and de Boer JF, Opt. Express 15, 2421 (2007). [PubMed: 19532479]
13. Wang H, Al-Qaisi MK, and Akkin T, Opt. Lett. 35, 154 (2010). [PubMed: 20081952]
14. Rivet S, Marques MJ, Bradu A, and Podoleanu A, Opt. Express 25, 14533 (2017). [PubMed: 28789039]
15. Fercher A, Hitzenberger C, Sticker M, Zawadzki R, Karamata B,and Lasser T, Opt. Express 9, 610 (2001). [PubMed: 19424297]
16. Moon S and Chen Z, Biomed. Opt. Express 9, 5280 (2018) [PubMed: 30460128]
17. Moon S, Qu Y, and Chen Z, Opt. Express 26, 7253 (2018). [PubMed: 29609412]

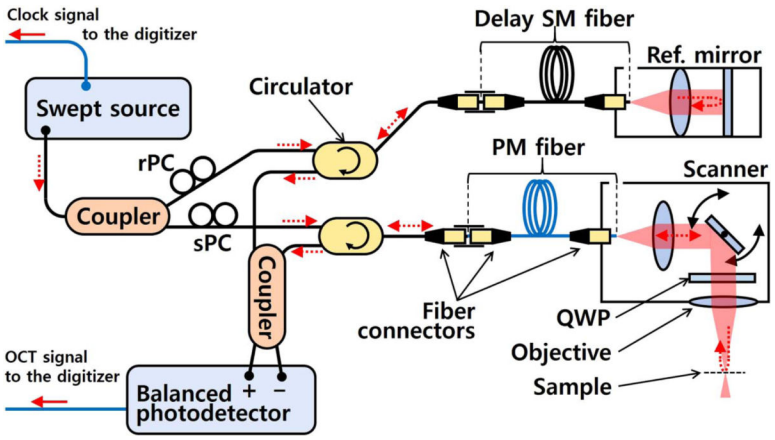

Fig. 1.

Schematic of our PS-OCT system. A long section of PM fiber is placed at the sample arm, while an SM fiber section of the same length is added at the reference arm. The rest of the fibers are all SM fibers.

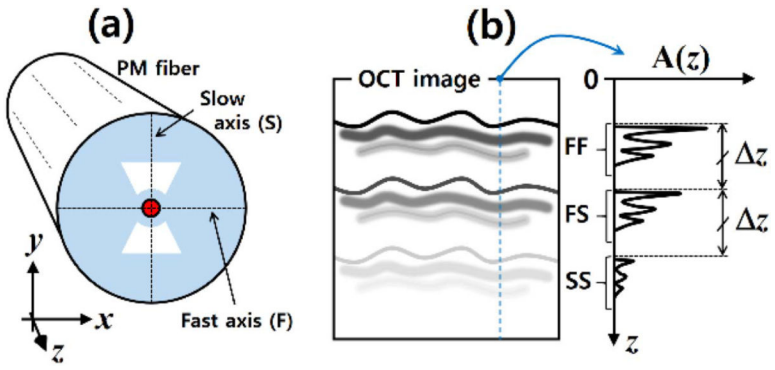

Fig. 2.

Definition of the coordinates with the PM fiber axes (a) and FF, FS, and SS image replicas obtained by our PS-OCT system (b).

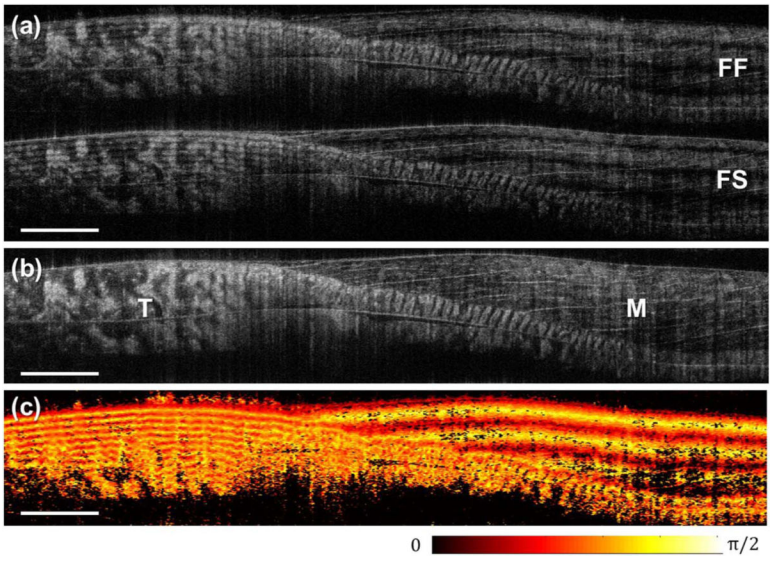

Fig. 3.

Images of rabbit tendon and muscle: the raw OCT image (a) contains FF and FS image segments separated by ~2.7mm. The normal image of reflectivity (b) and the map of sample-field retardation (c) were obtained by amplitude-based analysis given by Eqs. (7) and (8), respectively. T, tendon; M, muscle. Scale bar: 2 mm.